




Validation of GaoFen-1 Satellite Geometric Products Based on Reference Data

Qiyue Liu^{1,2} · Tao Yu¹ · Wenhao Zhang¹ 

Received: 26 December 2018 / Accepted: 21 June 2019 / Published online: 26 June 2019
© Indian Society of Remote Sensing 2019

Abstract

Applications of high-resolution remote sensing satellite data are becoming increasingly extensive. China has launched a series of high-resolution optical satellites: GaoFen-1 (GF-1), GaoFen-2, etc., and published several remote sensing image products. However, validation of the long time series of these satellite geometric products is lacking. Therefore, this study selects 2013–2016 GaoFen-1 satellite geometry products for the Beijing area over four years, obtaining a total of 164 images, and uses ZY-3 satellite products to verify the accuracy of the data set. Moreover, the positioning accuracy of the geometric products of two camera types carried by GF-1 (wide field of view, WFV; panchromatic and multispectral, PMS) is analyzed. The results yield the following conclusions. (1) GF-1 satellite geometric products have obvious systematic errors, and the error value varies significantly with the orbit time. (2) The internal distortion of the GF-1 satellite image is well controlled, and the geometric offset magnitude and direction of ground control points (GCPs) are very similar in the interior of each scene. (3) In a short period of time (20 days), the offset direction of the four WFV cameras is very similar, but there is a small difference in the mean plane offset (RMSE_{2D}). The RMSE_{2D} and offset direction of the two PMS cameras are very similar. (4) In the long term, the relative offset of the WFV and PMS cameras varies with the satellite orbit time. At the first year of the satellite orbit time (in 2014), the relative offsets of four WFV cameras increased to maximum (168.96 m, 171.12 m, 226.65 m, and 207.04 m). From 2015 to 2016, the offsets decreased to a relatively stable state (within 100 m). (5) This validation method based on reference data is shown to be feasible. This study provides an important reference for the application of high-resolution remote sensing satellite products.

Keywords Validation · GF-1 satellite · Geometric product · Positioning accuracy

Introduction

High-spatial-resolution (HSR) remote sensing satellites are playing an increasingly important role in global Earth observations. HSR satellite images, such as Landsat TM, QuickBird, Worldview, and SPOT series satellites, have been widely used in agricultural statistics, environmental monitoring, land utilization city change detection, and energy development (Battude et al. 2016; Samiappan 2017; Persson and Perko 2016; Li et al. 2015; Hamada et al.

2016; Tarantino et al. 2016; Zhang et al. 2017; Yan et al. 2016).

The geometric quality of HSR remote sensing satellite image products is an important index used to evaluate the quality of remote sensing images and reflect the technical level of the satellite sensor. Validating the geometric location quality of remote sensing satellite products is essential for supporting the operation and application of satellites (Huang et al. 2014). It has an important influence on quantitative remote sensing applications, such as surface object recognition, information extraction, and 3D reconstruction (Han 2015). However, due to the influence of gravity, atmosphere, mechanical wear, and topography, the change in the exterior and interior orientation elements of the sensor, resulting in a decline of geometric quality, impacts high-precision applications. Therefore, it is important to validate the geometric quality of remote

✉ Wenhao Zhang
Zhangwh@radi.ac.cn

¹ Institute of Remote Sensing and Digital Earth, Chinese Academy of Sciences, No. 20 North Datun Road, Chaoyang District, Beijing, China

² University of Chinese Academy of Sciences, Beijing, China

sensing satellite products to determine the attenuation of satellite sensors and improve parameters to ensure high-quality satellite images. Previously, Storey et al. made an on-orbit geometric calibration for the Landsat-8 satellite OLI camera and verified the geometric performance, including the absolute geodetic accuracy (CE90), the geometric (Level 1T product) accuracy (CE90), the band registration accuracy (LE90), and the image registration accuracy (LE90) (Chen 2015). Furthermore, Bouillon et al. presented an in-flight geometric characterization of SPOT-5 during the first two months of its orbit (Bouillon et al. 2003a, b; Storey et al. 2014), and Barazzetti et al. (2016) analyzed the georeferencing accuracy of a single WorldView-3 image collected over Milan.

In 2008, China implemented the China High-Resolution Earth Observation System (CHEOS) and launched a series of HSR satellites, such as GF-1 and GF-2. GF-1 is the first HSR satellite of CHEOS; its image products have been widely used in many industries (Li et al. 2015, 2017; Zheng et al. 2016; Wei et al. 2015; Chen 2015; Hao et al. 2015), and GF-1 image geometric quality has been thoroughly studied. Huang et al. 2016 validated the positioning accuracy of five GF-1 panchromatic and multispectral (PMS) images after ortho-rectification using the rational function model (RFM) (Battude et al. 2016); Song et al. (2016) used SPOT-5 images as reference data to test and analyze the geometric accuracy of one scene of GF-1 data; and Wang et al. (2016) used a geometric calibration method based on RFM to perform a geometric correction for 23 GF-1 wide-field-of-view (WFV) images from July 2013 to April 2014, before validating image positioning accuracy. However, these studies only used a small number of GF-1 images to analyze geometric performance, and the results only reveal GF-1 geometric quality for a certain time, which cannot reflect the positioning accuracy of GF-1 image products (Han 2015). Therefore, extensive long-term research on GF-1 satellite geometry quality is required. This can enable data users to fully understand GF-1 image geometric quality, which will improve the quality of data applications.

This study selected Beijing as the study area and performed a long-term geometric quality validation of GF-1 images. Firstly, 164 images (136 WFV and 28 PMS) were collected from the launch of the satellite (2013) to 2016, and systematic geometric correction based on the RFM model was conducted. Then, taking the ZY-3 satellite geometry product, which proved to have very high positioning accuracy (Huang 2013), as reference data, we selected GCPs in GF-1 and ZY-3 data and compared the geodetic coordinates to determine the relative positioning accuracy of GF-1, including the maximum error, minimum error, mean error, standard error, and root mean square error (RMSE). Finally, changes in the offset magnitude and

direction with on-orbit time of the GF-1 satellite were analyzed. This study will provide an important reference for subsequent remote sensing applications of HSR satellites and validation method of geometric products for other HSR satellites.

The structure of this paper is as follows: the motivation and background are described in “[Introduction](#)” section; the data and validation method are presented in “[Data and Methods](#)” section; the results are presented and discussed in “[Results and Discussion](#)” section; and conclusions are drawn in “[Conclusion](#)” section.

Data and Methods

Study Area

The study area is Beijing, the capital of China, extending from 115.7°E to 117.4°E longitude and 39.4°N to 41.6°N latitude (Fig. 1). The terrain in the study area mainly includes urban, farmland, and village.

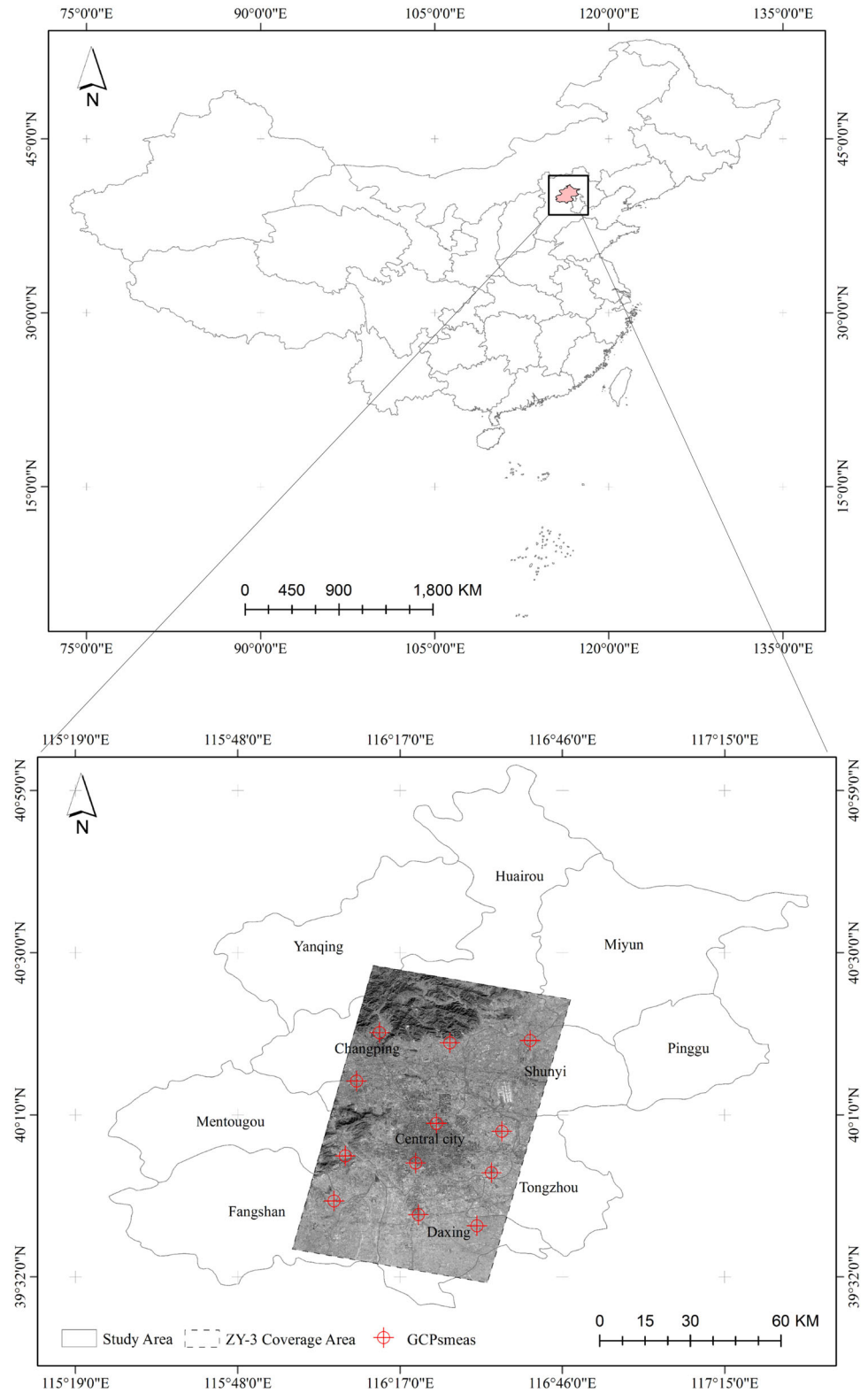
Data Preparation and Preprocessing

GF-1 Satellite Data

GF-1 is the first satellite of CHEOS, launched successfully in April 2013, equipped with two 2-m resolution panchromatic/8-m resolution PMS cameras and four 16-m resolution WFV cameras (CRESDA 2017; Bai 2013). PMS camera has five bands, namely panchromatic, blue, green, red and near-infrared bands. WFV camera has four bands, namely blue, green, red and near-infrared bands. The field of view (FOV) of the PMS camera’s panchromatic band is consistent with that of the other four bands. Therefore, the positioning accuracy of the 2 m panchromatic band data is not studied in this paper. GF-1 includes many key technologies such as a combination of high spatial resolution, multispectral, and wide coverage. Table 1 shows the information of GF-1 satellite.

The China Centre for Resource Satellite Data and Application (CRESDA 2017, the official operational management agency of GF-1 satellite) is responsible for the publishing of GF-1 satellite data, including WFV and PMS data in TIFF file format. To ensure the effectiveness of the verification, we collected GF-1 geometric products of the study area as much as possible. Then, the following strategies are applied to acquire the valid GF-1 images: (a) The GF-1 images must be clearly visible and less covered by clouds. (b) The overlap between GF-1 image data and reference data (ZY-3) should be as large as possible. (c) Try to collect the valid data in every month from 2013 to 2016 for each camera. Under these strategies, 164

Fig. 1 Location of the study area, ZY-3 coverage area, and $GCPs_{meas}$ ($GCPs_{meas}$ are represented in cross in a circle in red color, used for geometric correction of reference data (ZY-3) to further improve its positioning accuracy) (color figure online)



GF-1 satellite images from 2013 to 2016 were retrieved, including 136 WFV multispectral images (33 for WFV1, 34 for WFV2, 36 for WFV3, and 33 for WFV4), and 28

PMS multispectral images (8 for PMS1, 20 for PMS2). The information of the collected imagery is listed in Tables 2 and 3. Almost in every month there is at least one image,

Table 1 Sensor characteristics of the GF-1 satellite

Satellite	Sensor	Band name	Spectral channels (μm)	Spatial resolution (m)	Swath width (km)	Revisit period (day)
GF-1	PMS	Panchromatic	0.45–0.90	2	60	4
		Blue	0.45–0.52	8		
		Green	0.52–0.59			
		Red	0.63–0.69			
		Near infrared	0.77–0.89			
	WV	Blue	0.45–0.52	16	800	2
		Green	0.52–0.59			
		Red	0.63–0.69			
		Near infrared	0.77–0.89			

only few months lacking data due to the influence cloud coverage.

Reference Image Data

Chinese surveying and mapping satellite ZY-3 was used as reference data. On January 21, 2014, two sensor-corrected ZY-3 image products from the same orbit were acquired from the Satellite Surveying and Mapping Application Center, National Administration of Surveying, Mapping and Geoinformation of China (SASMAC, NASG) (SASMAC 2017) (Table 4). The ZY-3 satellite has higher positioning accuracy, which achieves a seamless mosaic between the CCDs, and the attached rational polynomial coefficient (RPC) parameters have high fitting accuracy and can replace the strict imaging model. Furthermore, the ZY-3 product has corrected the internal distortion of sensor (Pan et al. 2014; Zhang et al. 2013; Huang 2013; Wang et al. 2016).

In order to further improve the positioning precision of the reference data, 12 ground control points (GCPs_{meas}, as shown in Fig. 1) were measured with a differential global positioning system (DGPS), and geometric correction was performed on ZY-3 satellite image data using binary and polynomial modes (Pan et al. 2013). The geometric correction results show that the average plane positioning accuracy can reach 2.5 m, which is consistent with previous studies (Tang et al. 2012; Pan et al. 2013).

Data Preprocessing

The GF-1 image products obtained from CRESDA are level 1 products (relative radiation correction products); GF-1 systematic geometric correction image products are used as validation objects in this study. Therefore, in order to accurately choose GCPs, geometric correction of GF-1 images was performed based on the rational function

model (RFM) before selecting GCPs. The RFM model is a high-resolution satellite sensor imaging geometric model, which is widely used throughout the world. RFM describes the relationship between image point coordinates (x, y) and ground point coordinates (P, L, H), which have the following general form (Fraser and Hanley 2003):

$$\begin{cases} Y = \frac{p_1(P, L, H)}{p_2(P, L, H)} \\ X = \frac{p_3(P, L, H)}{p_4(P, L, H)} \end{cases} \quad (1)$$

In these equations, (X, Y) does not represent sample and line on the image, but regularized image coordinates from sample and line. They correspond to the ground point with object space coordinates (P, L, H), which are the variables of a polynomial p_i ($i = 1, 2, 3, 4$) of a degree not exceeding three. The form of the polynomial p_i ($i = 1, 2, 3, 4$) is:

$$\begin{aligned} p_i = & a_{(i,1)} + a_{(i,2)}L + a_{(i,3)}P + a_{(i,4)}H + a_{(i,5)}LP + a_{(i,6)}LH \\ & + a_{(i,7)}PH + a_{(i,8)}L^2 + a_{(i,9)}P^2 + a_{(i,10)}H^2 + a_{(i,11)}PLH \\ & + a_{(i,12)}L^3 + a_{(i,13)}LP^2 + a_{(i,14)}LH^2 + a_{(i,15)}L^2P \\ & + a_{(i,16)}P^3 + a_{(i,17)}PH^2 + a_{(i,18)}L^2H \\ & + a_{(i,19)}P^2H + a_{(i,20)}H^3 \end{aligned} \quad (2)$$

where $a_{(i,1)}, \dots, a_{(i,20)}$ are rational polynomial coefficients (RPCs), which can be obtained from incidental data of the GF-1 satellite.

GCPs Data

The GCPs are selected from the preprocessed GF-1 image and ZY-3 image data. The coverage area of each GF-1 WFV image and ZY-3 image is essentially the same; therefore, to ensure the reliability of validation results, six identical GCPs were selected from ZY-3 and GF-1 WFV images. The number of GCPs from PMS and ZY-3 images

Table 2 The information of GF-1 WFV data used to validation

WFV1			WFV2			WFV3			WFV4		
No.	Date	Scene ID	No.	Date	Scene ID	No.	Date	Scene ID	No.	Date	Scene ID
1	2013.09.07	120211	1	2013.05.05	8848	1	2013.06.03	32297	1	2013.07.30	88951
2	2013.09.11	122198	2	2013.08.30	115511	2	2013.07.17	79381	2	2013.12.14	185267
3	2013.09.27	131750	3	2013.09.15	124525	3	2013.07.25	86898	3	2013.12.26	193958
4	2013.10.17	142733	4	2013.11.27	177261	4	2013.08.10	101902	4	2013.12.30	196670
5	2013.12.09	181652	5	2013.12.05	178887	5	2013.10.26	151488	5	2014.02.05	223745
6	2014.01.10	205530	6	2013.12.13	184798	6	2013.11.03	153608	6	2014.03.01	244119
7	2014.03.04	247116	7	2014.02.04	223006	7	2013.11.07	155944	7	2014.04.03	276215
8	2014.05.21	326049	8	2014.03.29	270925	8	2013.11.11	158019	8	2014.06.28	371431
9	2014.06.27	370074	9	2014.06.23	365472	9	2014.01.15	210037	9	2014.08.12	428106
10	2014.08.07	421716	10	2014.08.15	433348	10	2014.01.27	217541	10	2014.09.18	496579
11	2014.08.11	426337	11	2014.09.09	475224	11	2014.03.01	244119	11	2014.10.17	563720
12	2014.11.05	613054	12	2014.10.16	561993	12	2014.05.05	318422	12	2014.11.02	605994
13	2014.11.09	623656	13	2015.01.02	777405	13	2014.06.07	348066	13	2015.01.11	801801
14	2014.12.04	696611	14	2015.01.06	789253	14	2014.07.10	385848	14	2015.01.19	824036
15	2014.12.16	766593	15	2015.01.10	800009	15	2014.11.18	659500	15	2015.02.17	915715
16	2014.12.24	747492	16	2015.03.25	1037362	16	2014.12.17	763892	16	2015.02.25	942498
17	2015.01.22	833576	17	2015.04.06	1078720	17	2014.12.25	751942	17	2015.05.18	1210349
18	2015.02.24	945456	18	2015.07.22	1428760	18	2015.01.31	863497	18	2015.05.26	1240122
19	2015.04.10	1089927	19	2015.07.26	1439208	19	2015.03.09	980119	19	2015.07.02	1359003
20	2015.04.14	1099764	20	2015.12.04	1841283	20	2015.03.17	1006857	20	2015.08.08	1480339
21	2015.04.22	1127946	21	2016.01.06	1966428	21	2015.04.23	1130640	21	2015.09.14	1591923
22	2015.05.25	1235878	22	2016.01.10	1979879	22	2015.08.20	1516944	22	2015.10.04	1653472
23	2015.06.02	1263484	23	2016.02.16	2107020	23	2015.08.28	1540418	23	2015.10.29	1733109
24	2015.08.15	1499840	24	2016.02.24	2135219	24	2015.09.26	1628739	24	2015.12.17	1884599
25	2015.10.24	1715064	25	2016.03.11	2191269	25	2015.10.08	1664816	25	2016.01.11	1986694
26	2015.11.01	1741523	26	2016.04.09	2292893	26	2015.10.12	1675872	26	2016.01.15	2000370
27	2016.01.18	2010098	27	2016.04.13	2301651	27	2015.11.02	1744417	27	2016.01.19	2016831
28	2016.03.11	2191246	28	2016.05.08	2387850	28	2016.01.02	1953226	28	2016.04.10	2292466
29	2016.04.21	2329683	29	2016.05.16	2413282	29	2016.01.31	2054707	29	2016.05.17	2417029
30	2016.05.28	2451859	30	2016.06.22	2535323	30	2016.02.08	2081022	30	2016.06.19	2522990
31	2016.08.26	2745175	31	2016.09.08	2790883	31	2016.03.24	2234531	31	2016.09.29	2853172
32	2016.09.20	2833971	32	2016.09.28	2848348	32	2016.04.22	2334829	32	2016.11.05	2984265
33	2016.11.16	3022513	33	2016.10.11	2894681	33	2016.04.30	2358825	33	2016.12.08	3099056
			34	2016.12.15	3123354	34	2016.05.29	2454699			
						35	2016.08.27	2747725			
						36	2016.12.16	3126904			

was 11, and because the swath width of the PMS camera is 60 km, the overlap area of different PMS images and ZY-3 data was quite different. Therefore, GCPs selected in different PMS images were not completely equivalent.

Some researches show that the accuracy of GCPs and its spatial distribution will affect the geometric correction results of remote sensing images (Tao et al. 2017). Obviously, in the validation of images positioning accuracy, the

error of GCPs will reduce accuracy and reliability of the validation results.

The possible error of GCPs in our method is mainly from the process of selecting corresponding points (You et al. 2011). To minimize this error, we take several methods. Firstly, we selected ZY-3 products as reference data, which has much higher spatial resolution (2 m) than GF-1 (PMS: 8 m; WFV: 16 m). Besides, as a satellite used

Table 3 The information of GF-1 PMS data used to validation

PMS1			PMS2					
No.	Date	Scene ID	No.	Date	Scene ID	No.	Date	Scene ID
1	2013.08.14	104408	1	2013.05.01	68662	11	2014.11.18	653869
2	2014.06.07	347262	2	2013.05.29	27368	12	2015.01.31	861627
3	2014.11.18	653740	3	2013.06.19	55458	13	2015.02.08	882849
4	2015.06.11	352149	4	2013.08.10	101299	14	2015.02.16	910744
5	2015.10.12	1674821	5	2013.08.14	104471	15	2015.05.05	1171407
6	2016.01.02	1952473	6	2014.01.19	212359	16	2015.10.12	1674420
7	2016.01.06	1965166	7	2014.01.27	217109	17	2016.01.02	1952592
8	2016.03.24	2233226	8	2014.04.27	299072	18	2016.03.24	2232861
			9	2014.05.05	306644	19	2016.08.27	2746306
			10	2014.06.07	347379	20	2016.09.04	2773963

Table 4 The information of ZY-3 data used as reference data

Satellite	Spatial resolution (m)	Date	Imaging time (UTC)	Data name
ZY-3	2.1	2014.01.21	03:17:52	ZY3_NAD_E116.4_N40.2_20140121_L1A0001677920
			03:17:58	ZY3_NAD_E116.3_N39.8_20140121_L1A0001548123

for surveying and mapping, ZY-3 was reported has very high positioning accuracy (Storey et al. 2014; Huang 2013; Tang et al. 2012; Pan et al. 2013) (1–2 pixels). Secondly, in this paper the corresponding points are from visual interpretation and artificial selecting. The error is controlled within one pixel, which ensures that GCPs have high accuracy to conduct the validation of positioning accuracy of remote sensing images.

Validation Method

According to Wu et al. (2015), the validation methods for remote sensing products are classified into: (a) validation based on a single-point ground measurement; (b) validation based on multi-point ground measurement; (c) validation based on high-resolution remote sensing data; (d) cross-validation; and (e) indirect validation. Nevertheless, this classification mainly relates to remote sensing land surface parameters, such as soil and vegetation, and does not include geometric parameters.

In this study, the validation method of remote sensing satellite geometry products is divided into two methods according to data source: (a) validation based on ground measured data and (b) validation based on reference image data. The main purpose of this study was to validate the relative geometric positioning accuracy of long time series GF-1 images; thus, validation data do not require very high absolute positioning accuracy. Therefore, method (b) was selected in this research.

Method (b) uses another satellite geometry product with high positioning accuracy as reference image validation data by comparing GCPs in the products and reference images. This method can be applied without ground measured data. The validation procedure is shown as follows:

- (1) The collection of GF-1 and reference satellite images, requiring high image quality and visual clarity.
- (2) Data preprocessing, including projection transformation and geometric correction.
- (3) GCPs selection in both GF-1 image products and reference images data following the principle of from left to right and from top to bottom. The GCPs must be well defined and homogeneously distributed on the image.
- (4) Error calculation (D) of GCPs:

$$D = \sqrt{\Delta X^2 + \Delta Y^2} \quad (3)$$

where $\Delta X = X_i - X_t$, $\Delta Y = Y_i - Y_t$, and X_i, X_t, Y_i, Y_t are horizontal and vertical coordinates of GCPs in GF-1 and reference data, respectively.

- (5) Root mean square error (RMSE_{2D}) calculation, defined as the geometric positioning accuracy of GF-1 satellite images, as follows:

$$\text{RMSE}_{2D} = \sqrt{\frac{\sum_{i=1}^n D_i^2}{n}} \quad (4)$$

where D_i is the error of point i , and n is the total number of GCP.

Results and Discussion

The geometric characteristics of a single GF-1 satellite image (WFV and PMS) and the variations of offset in magnitude and direction over time are analyzed in this section.

Offset Characteristics in Single GF-1 Images

Offset Characteristics of a Single WFV Camera Image

Firstly, the positioning accuracy and offset characteristics of the same WFV image scene are analyzed. One scene from each of the four WFV cameras is selected with an imaging time of within 20 days, on June 27, June 23, July 10, and June 28, 2014, respectively. The results show that the geometric offset of the GCPs is almost the same in both magnitude and direction (Fig. 2). Furthermore, the offset

magnitude and direction of the four WFV images are very similar. On a short timescale, compared with the reference data, the offset characteristics of the four cameras are essentially equivalent.

Table 5 shows the maximum error, minimum error, mean error, standard error, and RMSE_{2D} of the four WFV images. The RMSE_{2D} for WFV 1–4 is 138.05 m, 127.58 m, 178.44 m, and 160.24 m, respectively. Although the RMSE_{2D} values are close and the imaging time is within 20 days, it is notable that the RMSE_{2D} is more similar between WFV1 and WFV2 and between WFV3 and WFV4. In general, the difference in the RMSE_{2D} between the four images is within three pixels.

Offset Characteristics of a Single PMS Camera Image

The internal geometric offset magnitude and direction for the PMS camera image are almost the same for both PMS1

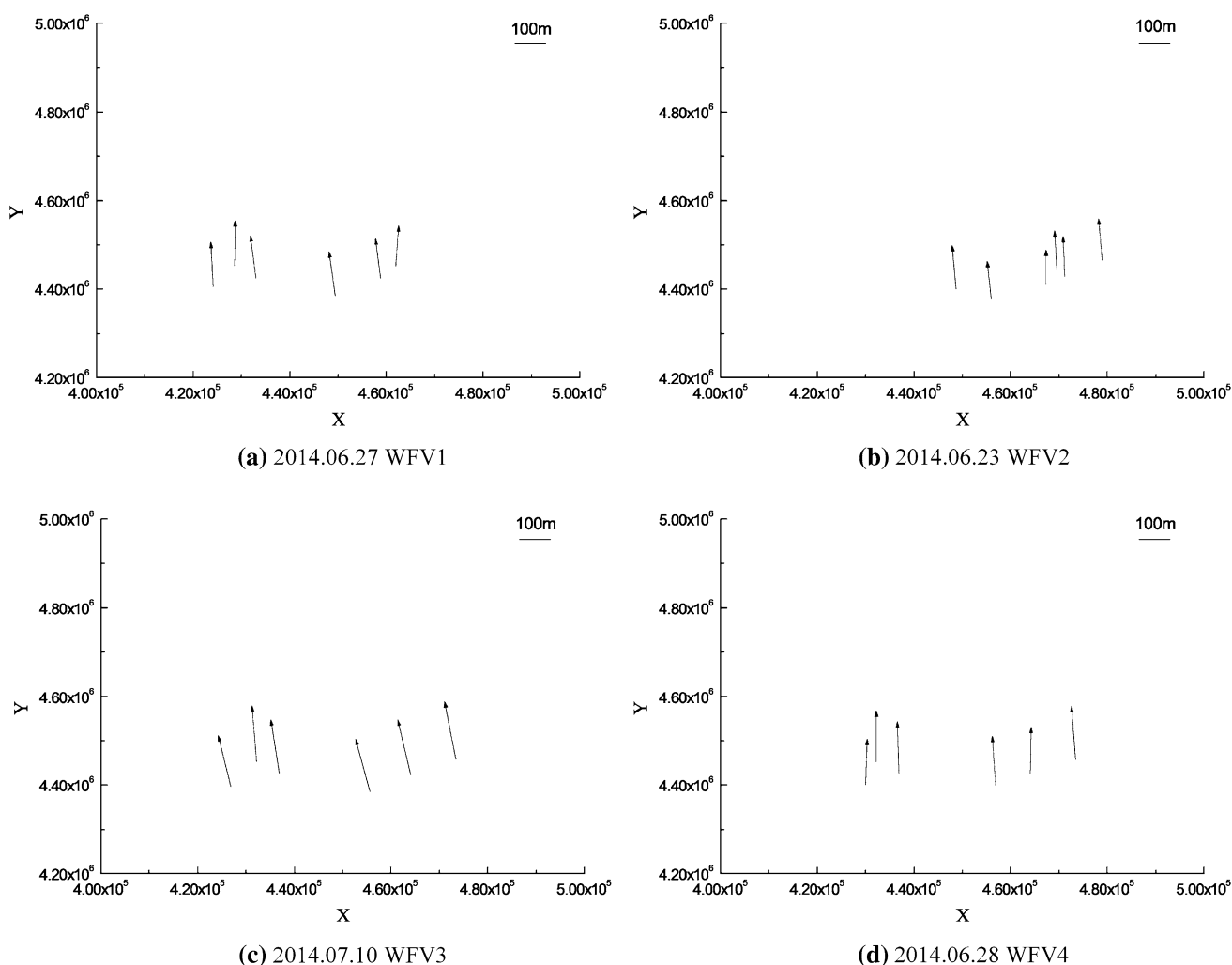


Fig. 2 Offset characteristics of a single WFV camera image. The starting position of the arrow in the graph represents the X and Y coordinates (UTM coordinate system) of the GCPs in the RFM-

corrected images. The direction and length of the arrow indicate the direction and offset of the GCPs, respectively

Table 5 Statistical results of the offset of a single WFV camera

Date	Sensor	Maximum error (m)		Minimum error (m)		Mean error (m)		Standard error (m)		RMSE _{2D} (m)
		X _{max}	Y _{max}	X _{min}	Y _{min}	X _{mean}	Y _{mean}	X _{std}	Y _{std}	
2014.06.27	WFV1	143.92	8.57	128.45	-19.84	137.36	-8.58	6.39	10.76	138.05
2014.06.23	WFV2	140.91	0.72	111.62	-13.24	127.23	-8.24	9.18	4.73	127.58
2014.07.10	WFV3	185.8	-14.74	164.06	-44.73	174.82	-34.08	7.22	10.45	178.44
2014.06.28	WFV4	171.51	4.66	148.45	-12.73	160.09	-3.60	8.022	6.59	160.24

RMSE_{2D} indicates the accuracy of plane positioning

and PMS2 data (Fig. 3). Furthermore, there is no significant difference in the offset magnitude and direction between two images. (Both are acquired on August 10, 2014.) The maximum error, minimum error, mean error, standard error, and RMSE_{2D} of the two PMS images are presented in Table 6. The mean plane offsets (RMSE_{2D}) are very close (43.57 m and 39.23 m), with a difference within two pixels. The difference of RMSE_{2D} between two PMS images is less than two pixels (43.57 m and 39.23 m), indicating that the positioning accuracy is similar with each other.

Long-Term Offset Variations

Long-Term Variation of WFV Image Offsets

To analyze the location accuracy of each WFV camera, the mean plane offsets of all GCPs in each image are counted (Fig. 4). Figure 4 shows that with an increase in the orbit time of the GF-1 satellite, the offset of the four WFV cameras changes constantly. The shape of the change curves of the four cameras is similar, and all increase at first and then decrease, before becoming relatively stable.

In addition, the trend lines (red lines) clearly show that all four offsets are gradually declining.

The maximum error, minimum error, mean error, and RMSE_{2D} of the four cameras in the four years are presented in Table 7. The trends are very similar to those presented in Table 5, whereby the maximum RMSE_{2D} of WFV1 is close to that of WFV2 (168.96 m and 171.12 m, respectively), and that of WFV3 is close to that of WFV4 (226.65 m and 207.04 m, respectively). The mean RMSE_{2D} shows the same trend (72.24 m, 66.04 m, 81.33 m, and 81.72 m for WFV 1–4, respectively).

To compare and analyze the offset variations of the four WFV cameras, a quarterly averaged statistical graph of their relative offsets is presented in Fig. 5, indicating strong similarities between the four WFV cameras. However, in 2013, there are significant differences in the quarterly average offset between the four cameras, especially in the third quarter (minimum 20.58 m, maximum 120.35 m). This indicates that, during the commissioning period following its launch, the geometric consistency between the four cameras was poor and the prelaunch calibration parameters should be refined. Nevertheless, in the fourth quarter, the quarterly average offsets of the four

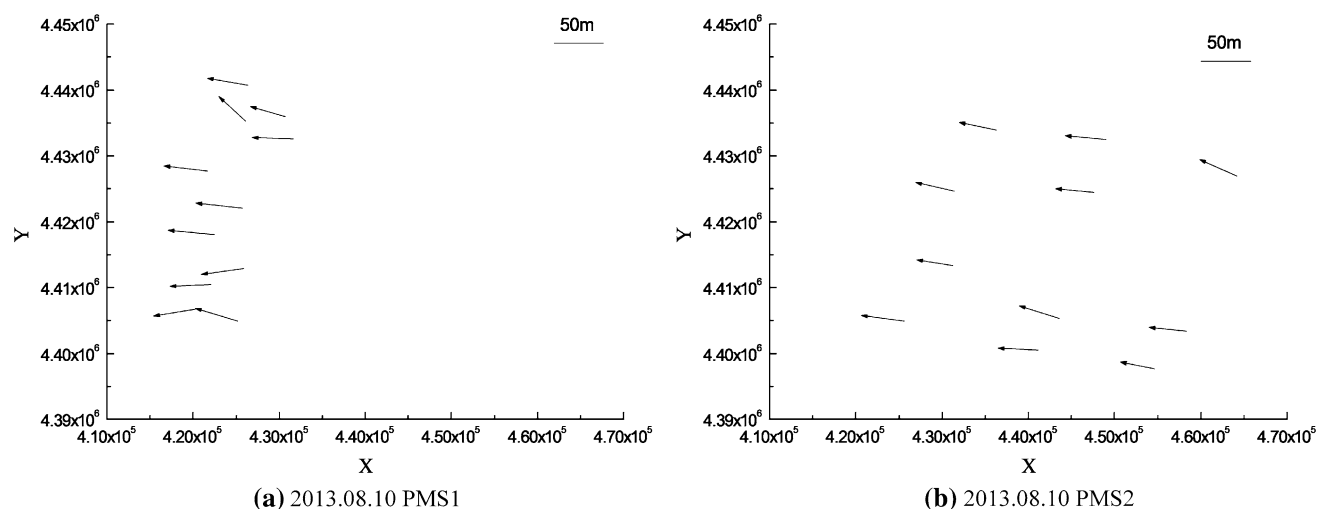


Fig. 3 Offset characteristics of a single PMS camera image. The starting position of the arrow in the graph represents the X and Y coordinates (UTM coordinate system) of the GCPs in the RFM-

corrected images. The direction and length of the arrow indicate the direction and offset of the GCPs, respectively

Table 6 Statistical results of the offset of a single PMS camera

Date	Sensor	Maximum error (m)		Minimum error (m)		Mean error (m)		Standard error (m)		RMSE _{2D} (m)
		X _{min}	Y _{min}	X _{min}	Y _{min}	X _{mean}	Y _{mean}	X _{std}	Y _{std}	
2013.08.10	PMS1	23.52	- 27.00	- 7.41	- 47.18	4.72	- 41.3	8.23	5.54	42.57
	PMS2	15.76	- 34.05	2.023	- 43.01	6.80	- 38.43	3.94	2.41	39.23

RMSE_{2D} indicates the accuracy of plane positioning

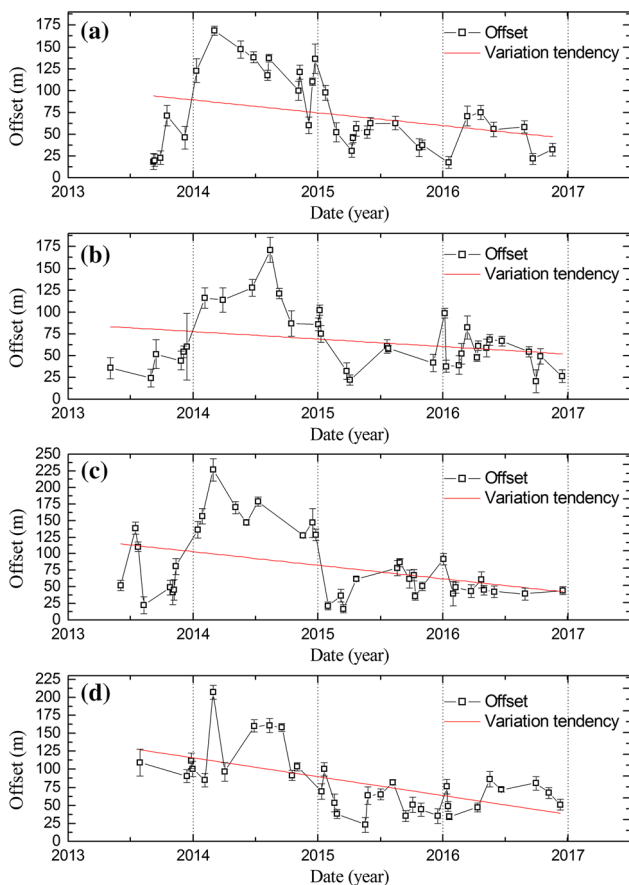


Fig. 4 The trends of four WFV camera offsets: **a** WFV1, **b** WFV2, **c** WFV3, and **d** WFV4. Red line is the trend line (color figure online)

cameras are very close (WFV1 = 58.55 m, WFV2 = 52.83 m, WFV3 = 54.20 m, and WFV4 = 66.95 m), and the geometric consistency and positioning accuracy are clearly improved. This is because the geometric calibration

parameters were updated after the on-orbit commissioning period. However, in 2014, except for the fourth quarter, all quarterly average offset values are above 100 m, the maximum of the four-year period. The geometric performance of the cameras therefore increases in the second year after launch. After the third quarter of 2014, the quarterly average offset values decline gradually. In 2015 and 2016, the geometric performance of the cameras is relatively stable; there are no significant changes in these two years, and all maximum offsets are within 100 m. This is because the satellite operation department conducted a second on-orbit geometric calibration and refined the satellite system parameters. Moreover, attenuation of the satellite camera stabilized.

Long-Term Variations of PMS Image Offsets

The offset trends of the two PMS cameras (PMS1 and PMS2) are shown in Fig. 6. The main aim of this paper is to analyze the geometric performance of GF-1 satellite geometry products. Although it seems that the amount of GF-1 PMS data in the study area is too small to draw a very reliable conclusion about the long-term trends of PMS geometry product positioning accuracy. However, from the available data we can see the obvious offsets fluctuations. The offsets of both cameras vary significantly with the on-orbit time since the launch. The minimum and maximum offsets of the PMS1 are 12.33 m and 69.21 m, and of the PMS2 are 8.11 m and 78.94 m, respectively. Moreover, the minimum and maximum offsets of the PMS1 and PMS2 camera are both appeared in 2014 and 2015. In the future research, we will select more study areas and longer time to get more data, thereby further analyzing the changing characteristics of PMS cameras.

Table 7 Maximum and mean errors of the four cameras

Sensor	Maximum error (m)		Minimum error (m)		Mean error (m)		RMSE _{2D}		
	X _{max}	Y _{max}	X _{min}	Y _{min}	X _{mean}	Y _{mean}	Max	Min	Mean
WFV1	151.39	37.52	- 41.85	- 74.72	66.02	18.91	168.96	17.61	72.74
WFV2	170.98	90.51	- 49.63	- 24.46	54.55	24.94	171.12	20.52	66.04
WFV3	201.51	103.48	- 134.71	- 34.08	67.29	29.50	226.65	16.57	81.33
WFV4	175.73	108.68	- 72.94	- 34.82	67.04	30.01	207.04	22.82	81.72

RMSE_{2D} indicates the accuracy of plane positioning

Fig. 5 Quarterly variation statistics of WFV camera offsets

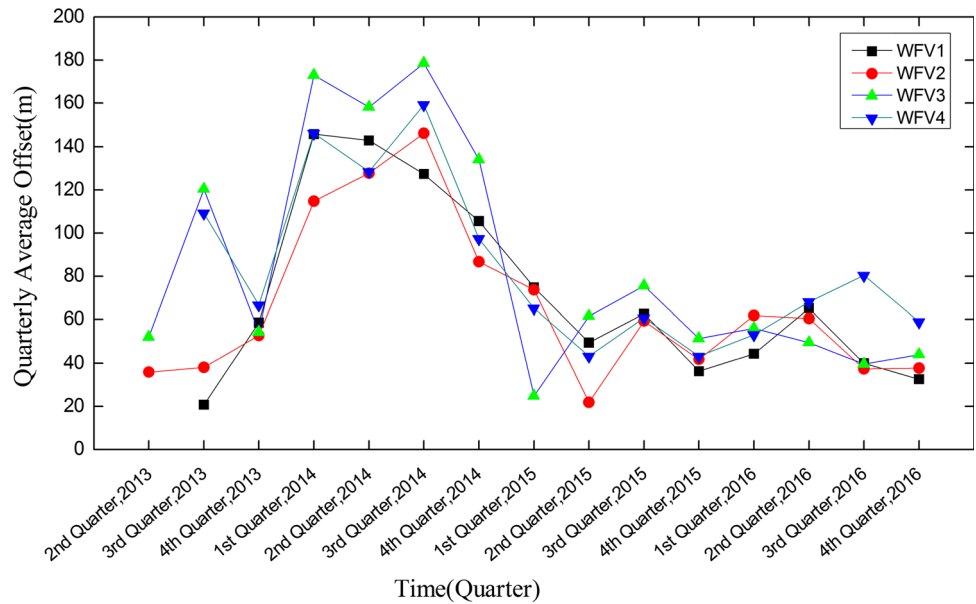
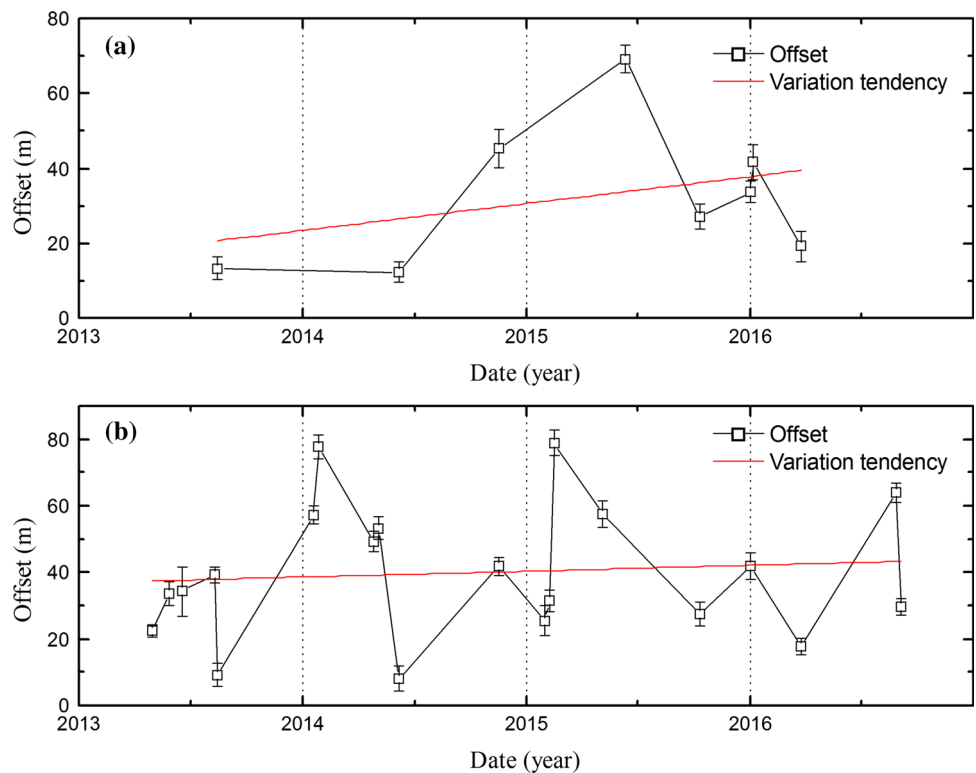


Fig. 6 The trends of two PMS camera offsets: **a** PMS1 and **b** PMS2. Red line is the trend line (color figure online)



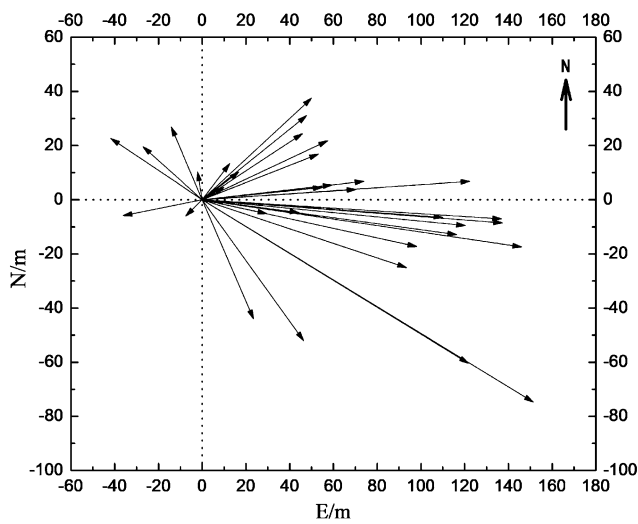
Long-Term Variations of Offset Direction

Offset Direction Statistics

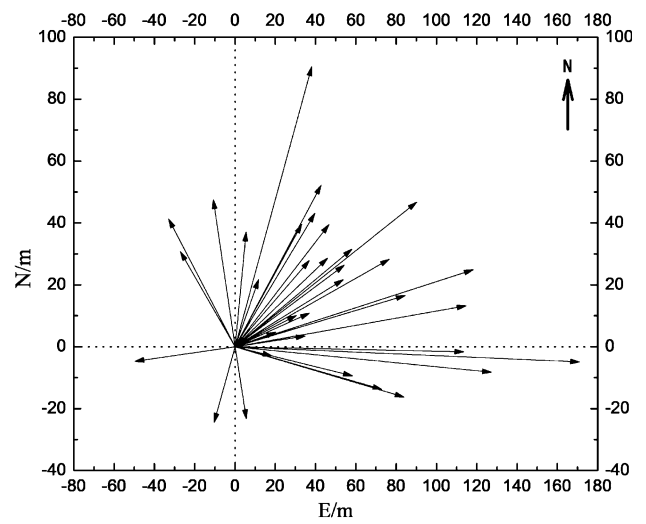
The statistics of the offset direction of the GF-1 WFV and PMS camera products are shown in Fig. 7. The length and direction of the arrow represent the magnitude and direction of the offset, respectively. And each arrow in the figure represents the average offset and direction of all the

GCPs in an image. The offset directions and magnitudes for the four WFV cameras are not fixed but show complex randomness and no clear trends (Fig. 7a–d). Therefore, if there is significant systematic deviation in the WFV camera

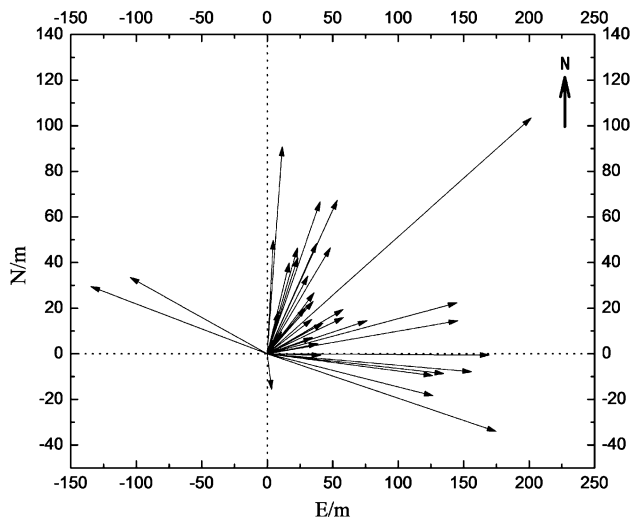
Fig. 7 Offset direction statistics for WFV and PMS camera products, each arrow represents the average offset and offset direction of all the GCPs in an image



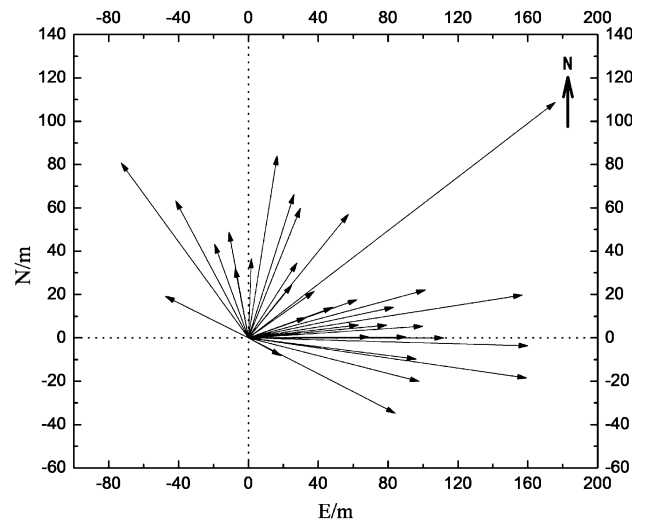
(a) WFV1



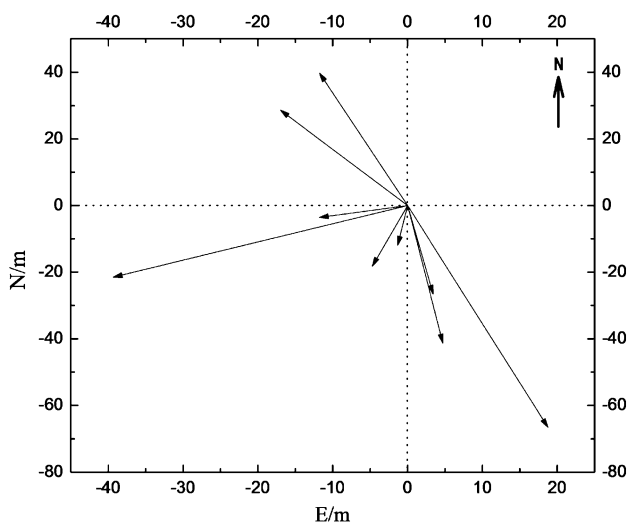
(b) WFV2



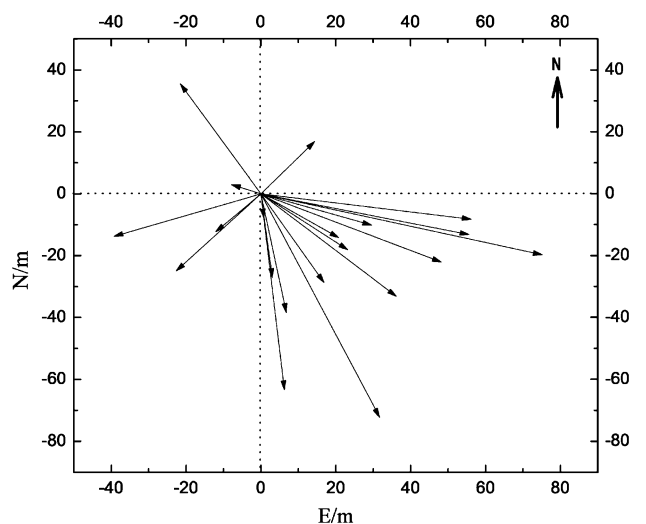
(c) WFV3



(d) WFV4



(e) PMS1



(f) PMS1

images, and we use the generalized image model compensation method to eliminate the system error, the RPC compensation parameter of a phase has no effect on the other phase images. On the other hand, more WFV images have offsets in the northeast direction than in other directions. Unlike the WFV camera, the PMS2 camera is clearly biased toward the southeast (Fig. 7f), while the offset direction feature is not obvious (Fig. 7e).

Offset Direction Trends

In Fig. 8, the quarterly features of the four WFV cameras are presented to reveal the variation in offset deviations. As

shown in Fig. 8, the following results can be drawn. (1) Except for the third quarter of 2015, the offset deviation for the four WFV cameras in the GF-1 satellite is inconsistent and shows clear differences. (2) In 2013, the satellite was in its commissioning period following launch, and the satellite systematic parameters were not stable, so the offset deviation of the four cameras changed sharply. (3) In 2014, the orientation of all cameras shifted to the southeast and northeast and was not biased toward the northwest and southwest. (4) In 2015 and 2016, the directions of the four cameras were both in the northeast and a little toward the northwest. Except for the first quarter of 2015, there were

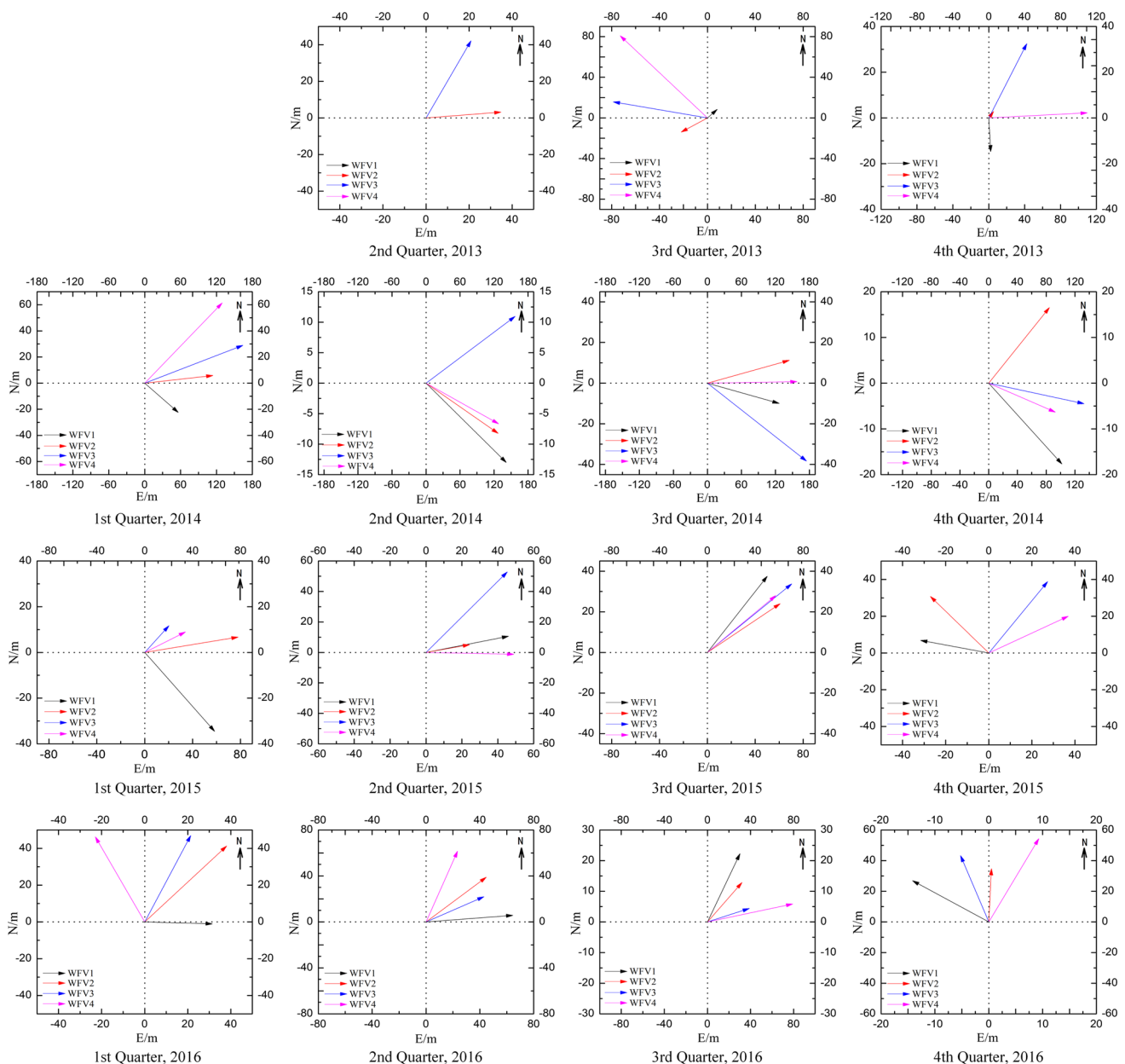


Fig. 8 Quarterly variations in the offset deviations of WFV cameras

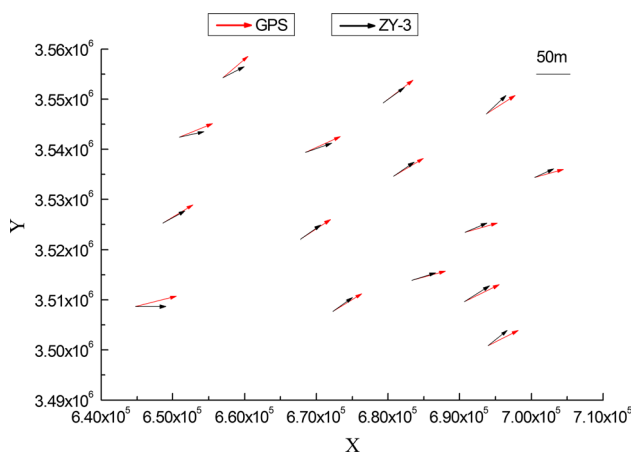


Fig. 9 Offset magnitude and direction using ZY-3 and GPS data (color figure online)

few WFV images with southeast and southwest offset directions.

Accuracy and Feasibility of the Validation Method

To verify the accuracy and feasibility of the validation method for geometric product location accuracy used in this study, a GF-1 WFV3 image product was selected in Nanjing, Jiangsu, eastern China, on April 21, 2016. The positioning accuracy of this WFV3 product was then validated using the ZY-3 geometric product data and 15 GPS control points.

Figure 9 shows result by two methods, from which we can see that the validated geometric offsets of WFV3 product based on ZY-3 image product (black arrow) are very similar to that using GPS data (red arrow). Furthermore, the offset direction results are generally the same for both datasets.

Table 8 shows the maximum error, minimum error, mean error, standard error, and RMSE_{2D} for WFV3 product positioning accuracy validation using ZY-3 and GPS data. The mean errors are 37.97 m and 52.78 m, respectively. Therefore, the accuracy of using ZY-3 data for geometric product validation is 71.94%. The accuracy is defined as (RMSE_{2D} by using ZY-3 sensor/RMSE_{2D} by using GPS) %.

Table 8 Validation precision using ZY-3 and GPS data

Data	Maximum error (m)		Minimum error (m)		Mean error (m)		Standard error (m)		RMSE _{2D} (m)
	X _{max}	Y _{max}	X _{min}	Y _{min}	X _{mean}	Y _{mean}	X _{std}	Y _{std}	
ZY-3	27.04	46.01	0.32	27.83	17.38	32.77	6.82	4.77	37.97
GPS	34.17	60.89	12.06	37.13	24.03	46.30	6.70	5.37	52.78

RMSE_{2D} indicates the accuracy of plane positioning

Figure 9 and Table 8 prove that the method used in this study provides comparable results to those using field measured GPS data. In addition, the method used in this paper has the advantage of low cost (labor, economic, time, etc.), fast, simple, free from time and place restrictions. Particularly, it does not require field measurement GCPs. Therefore, it is feasible for validating the long-term relative positioning accuracy of remote sensing satellite geometric products with reference satellite data. Besides, the method shown in this paper is also applicable to the validation of geometric products of other satellites.

Conclusion

From the geometric performance validation of four-year GF-1 satellite geometric products, the following conclusions can be drawn:

- (1) The geometric performance of four WFV cameras has changed with orbit time, and there are substantial differences in different cameras. In the early stage of satellite launch (2013 and 2014), the geometric positioning accuracy of the GF-1 WFV image product has clearly declined, while it improved in the year of 2015 and 2016. Therefore, it is necessary to perform on-orbit geometric calibration to eliminate the system error and improve the geometric quality of GF-1 image products.
- (2) The geometric offset magnitude and direction of GCPs are essentially equivalent for all GF-1 satellite images, regardless of WFV or PMS cameras, which indicates good internal distortion control of GF-1 satellite images. Over a short period of time (20 days), the offset direction of the four WFV cameras remains generally equal, but some difference is observed in the mean plane offset.
- (3) Over the four years, the relative offset of the WFV and PMS cameras varies with the orbit time of the satellite. The relative offset of the four WFV cameras increases at first, then decreases, and finally becomes relatively stable. In 2014, the offset values for all four cameras reached their maximum (168.96 m, 171.12, 226.65, and 207.04 m, respectively), and they were all within 100 m from 2015 to

2016. It is noteworthy that the maximum offset of WFV1 is similar to that of WFV2, while that of WFV3 is similar to that of WFV4; the reason for this phenomenon requires further study. The minimum and maximum offsets of the PMS1 and PMS2 cameras both occurred in 2014 and 2015 and they are 12.33 m and 69.21 m, and 8.11 m and 78.94 m, respectively, while the offset directions of WFV and PMS cameras vary substantially with time. WFV cameras are clearly biased toward the northeast, while PMS cameras are offset toward the southeast and southwest.

- (4) It is clear that the geometric performance of GF-1 satellite cameras is not consistent for the same

camera type, even if the camera is carried on the same satellite.

- (5) Validation using reference data is shown to be a feasible validation method.

Appendix: The Design Diagram and Observation Diagram of GF-1 WFV and PMS Sensor

The design and observation of the GF-1 WFV (four) and PMS (two) cameras are shown in Figs. 10, 11.

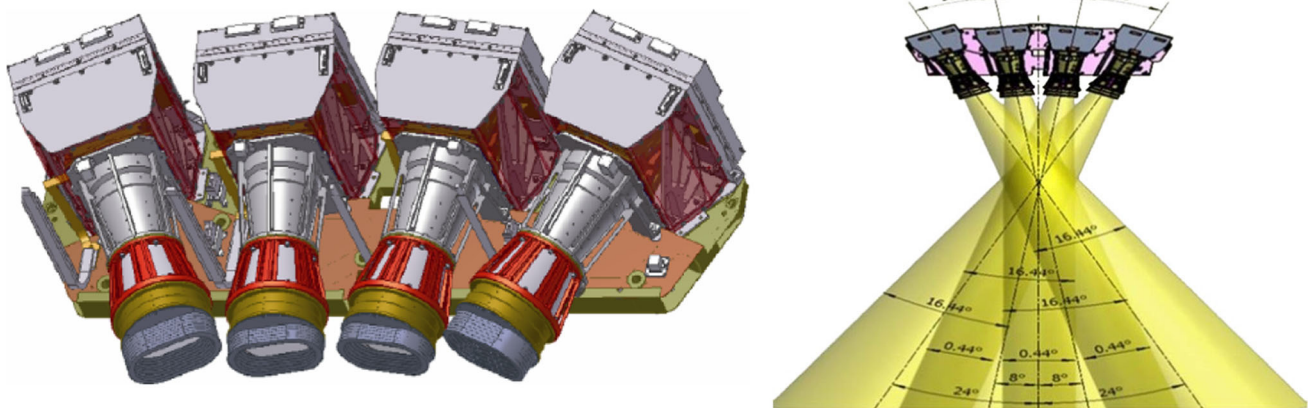


Fig. 10 The design diagram (left) and observation diagram (right) of the GF-1 WFV camera

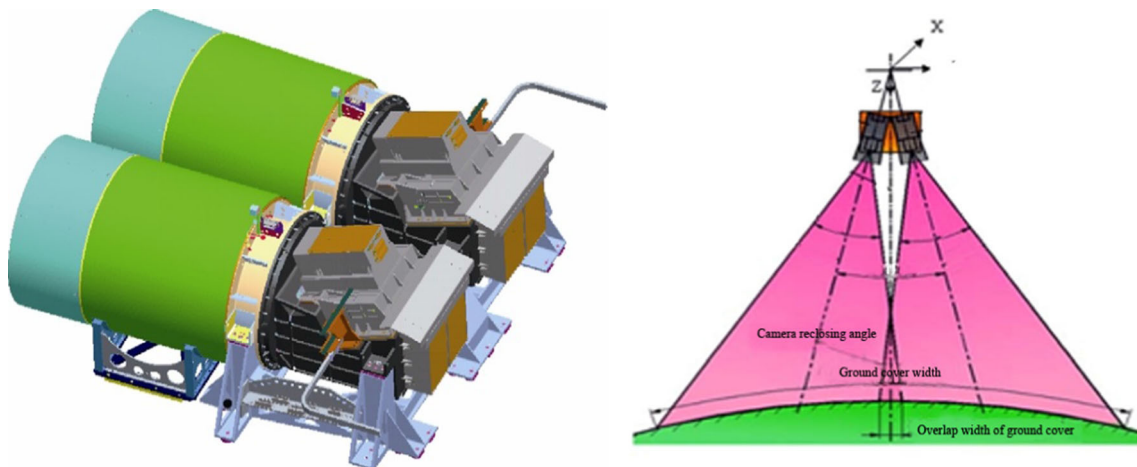


Fig. 11 The design diagram (left) and observation diagram (right) of the GF-1 PMS camera

References

- Bai, Z. (2013). Gao Fen-1 satellite's technical characteristic. *Aerospace China*, 1, 5–9.
- Barazzetti, L., Roncoroni, F., Brumana, R., & Previtali, M. (2016). Georeferencing accuracy analysis of a single WORLDVIEW-3 image collected over Milan. *The International Archives of the Photogrammetry, Remote Sensing and Spatial Information Sciences*, 41, 429–434.
- Battude, M., et al. (2016). Estimating maize biomass and yield over large areas using high spatial and temporal resolution Sentinel-2 like remote sensing data. *Remote Sensing of Environment*, 184, 668–681. <https://doi.org/10.1016/j.rse.2016.07.030>.
- Bouillon, A., et al. (2003a). SPOT5 HRG and HRS first in-flight geometric quality results. *International Symposium on Remote Sensing*, 4881, 212–223. <https://doi.org/10.1117/12.462637>.
- Bouillon, A., et al. (2003b). SPOT5 geometric image quality. *Geoscience and Remote Sensing Symposium*, 1, 303–305.
- Chen, N. (2015). Quantitative evaluation of observation capability of GF-1 wide field of view sensors for soil moisture inversion. *Journal of Applied Remote Sensing*, 9(1), 199–203. <https://doi.org/10.1117/1.JRS.9.097097>.
- CRESDA. (2017). China centre for resources satellite data and application. <http://www.cresda.com/-n16/index.html>.
- Fraser, C. S., & Hanley, H. B. (2003). Bias compensation in rational functions for Ikonos satellite imagery. *Photogrammetric Engineering and Remote Sensing*, 69(1), 53–57. <https://doi.org/10.14358/pers.69.1.53>.
- Hamada, Y., et al. (2016). Mapping ephemeral stream networks in desert environments using very-high-spatial-resolution multi-spectral remote sensing. *Journal of Arid Environments*, 130, 40–48. <https://doi.org/10.1016/j.jaridenv.2016.03.005>.
- Han, J. (2015). Study on the high precision geometric processing of GF-1 satellite images. *Stability analysis of geometric positioning of GF-1 satellite* (Vol. 2, pp. 25–26). Beijing: Institute of Remote Sensing and Digital Earth, Chinese Academy of Sciences.
- Hao, P., Wang, L., & Niu, Z. (2015). Potential of multitemporal Gaofen-1 panchromatic/multispectral images for crop classification: case study in Xinjiang Uygur Autonomous Region, China. *Journal of Applied Remote Sensing*, 9(1), 096035. <https://doi.org/10.1117/1.JRS.9.096035>.
- Huang, X. (2013). Quality assessment of panchromatic and multi-spectral image fusion for the ZY-3 satellite: from an information extraction perspective. *IEEE Geoscience and Remote Sensing Letters*, 11(4), 753–757. <https://doi.org/10.1109/lgrs.2013.2278551>.
- Huang, S., et al. (2014). Validation of positioning accuracy of GF-1 PMS images. *Spacecraft Recovery & Remote Sensing*, 35(5), 81–87.
- Huang, S., et al. (2016). Ortho accuracy validation and analysis on multispectral imagery of GF-1. *Science of Surveying and Mapping*, 41(3), 54–57.
- Li, W., et al. (2015a). Geostatistical modeling using lidar-derived prior knowledge with Spot-6 data to estimate temperate forest canopy cover and above-ground biomass via stratified random sampling. *International Journal of Applied Earth OBS*, 41, 88–98. <https://doi.org/10.1016/j.jag.2015.04.020>.
- Li, J., et al. (2015b). Improved capabilities of the Chinese high-resolution remote sensing satellite GF-1 for monitoring suspended particulate matter (SPM) in inland waters: Radiometric and spatial considerations. *ISPRS Journal of Photogrammetry and Remote Sensing*, 36, 145–156. <https://doi.org/10.1016/j.isprsjrs.2015.05.009>.
- Li, H., et al. (2017). Comparative analysis of GF-1, HJ-1, and Landsat-8 data for estimating the leaf area index of winter wheat. *Journal of Integrative Agriculture*, 16(2), 266–285.
- Pan, H., et al. (2013). Accuracy analysis and verification of ZY-3 products. *Acta Geodaetica et Cartographica Sinica*, 42(5), 738–751.
- Pan, H., et al. (2014). The geometrical model of sensor corrected products for ZY-3 satellite. *Acta Geodaetica et Cartographica Sinica*, 42(4), 516–522.
- Persson, H. J., & Perko, R. (2016). Assessment of boreal forest height from WorldView-2 satellite stereo images. *Remote Sensing Letters*, 7(12), 1150–1159. <https://doi.org/10.1080/2150704X.2016.1219424>.
- Samiappan, S. (2017). Using unmanned aerial vehicles for high-resolution remote sensing to map invasive *Phragmites australis* in coastal wetlands. *International Journal of Remote Sensing*, 38(8–10), 2199–2217. <https://doi.org/10.1080/01431161.2016.1239288>.
- SASMAC. (2017). NASG, Satellite Surveying and Mapping Application Center, National Administration of Surveying, Mapping and Geoinformation of China. http://www.sasmac.cn/portal_space/.
- Song, M., et al. (2016). Test and analysis of GF-11 satellite remote sensing data. *Inner Mongolia Science Technology & Economy*, 2, 84–86.
- Storey, J., Choate, M., & Lee, K. (2014). Landsat 8 operational land imager on-orbit geometric calibration and performance. *Remote Sensing*, 6(11), 11127–11152. <https://doi.org/10.3390/rs6111127>.
- Tang, X., et al. (2012). Triple linear-array imaging geometry model of Ziyuan-3 surveying satellite and its validation. *International Journal of Image & Data Fusion*, 4(1), 33–51.
- Tao, W., et al. (2017). Effect of precision of control points on geometric correction of remote sensing image. *Journal of North China University of Science and Technology(Natural Science Edition)*, 39(4), 7–14.
- Tarantino, C., et al. (2016). Detection of changes in semi-natural grasslands by cross correlation analysis with worldview-2 images and new Landsat 8 data. *Remote Sensing of Environment*, 175, 65–72. <https://doi.org/10.1016/j.rse.2015.12.031>.
- Wang, T., et al. (2016a). Combined calibration method based on rational function model for the Chinese GF-1 wide-field-of-view imagery. *Photogrammetric Engineering and Remote Sensing*, 82(4), 291–298. <https://doi.org/10.14358/pers.82.4.291>.
- Wang, M., et al. (2016b). Correction of ZY-3 image distortion caused by satellite jitter via virtual steady reimaging using attitude data. *ISPRS Journal of Photogrammetry and Remote Sensing*, 119, 108–123. <https://doi.org/10.1016/j.isprsjrs.2016.05.012>.
- Wei, C., et al. (2015). Monitoring of “Urban Villages” in Shenzhen, China from high-resolution GF-1 and TerraSAR-X data. *Proceedings of SPIE*, 9642, 964210. <https://doi.org/10.1117/12.2194877>.
- Wu, X., et al. (2015). Advances in validation methods for remote sensing products of land surface parameters. *Journal of Remote Sensing*, 19(1), 75–92.
- Yan, S., et al. (2016). Large deformation monitoring over a coal mining region using pixel-tracking method with high-resolution Radarsat-2 imagery. *Remote Sensing Letters*, 7(3), 219–228. <https://doi.org/10.1080/2150704X.2015.1126683>.
- You, S., et al. (2011). GCP error propagation model for geometric correction and its application. *Journal of Image & Graphics*, 16(3), 469–473.
- Zhang, Y., et al. (2013). On-orbit geometric calibration of ZY-3 three-line array imagery with multistrip data sets. *IEEE Transactions*

- on *Geoscience and Remote Sensing*, 52(1), 224–234. <https://doi.org/10.1109/TGRS.2013.2237781>.
- Zhang, X., et al. (2017). Separate segmentation of multi-temporal high-resolution remote sensing images for object-based change detection in urban area. *Remote Sensing of Environment*, 201, 243–255. <https://doi.org/10.1016/j.rse.2017.09.022>.
- Zheng, X., et al. (2016). Remote sensing monitoring of green tide in the Yellow Sea in 2015 based on GF-1 WFV data. *Proceedings of SPIE*, 9975, 99750L. <https://doi.org/10.1117/12.2235833>.

Publisher's Note Springer Nature remains neutral with regard to jurisdictional claims in published maps and institutional affiliations.